Journal of Power Sources 185 (2008) 676–684

Contents lists available at ScienceDirect

Journal of Power Sources

journal homepage: www.elsevier.com/locate/jpowsour

Structure and electrochemical properties of activated polyacrylonitrile based carbon fibers containing carbon nanotubes

Sudhakar Jagannathan, Han Gi Chae, Rahul Jain, Satish Kumar*

School of Polymer, Textile and Fiber Engineering, Georgia Institute of Technology, Atlanta, GA 30332, United States

ARTICLE INFO

Article history:
Received 3 July 2008
Received in revised form 27 August 2008
Accepted 28 August 2008
Available online 7 September 2008

Keywords:
Activated carbon
Polyacrylonitrile
Electrochemical capacitor
Carbon nanotubes

ABSTRACT

Solution spun polyacrylonitrile (PAN), PAN/multi-wall carbon nanotube (MWCNT), and PAN/single-wall carbon nanotube (SWCNT) fibers containing 5 wt.% carbon nanotubes were stabilized in air and activated using CO_2 and KOH. The surface area as determined by nitrogen gas adsorption was an order of magnitude higher for KOH activated fibers as compared to the CO_2 activated fibers. The specific capacitance of KOH activated PAN/SWCNT samples was as high as 250 F g^{-1} in 6 M KOH electrolyte. Under the comparable KOH activation conditions, PAN and PAN/SWCNT fibers had comparable surface areas (BET surface area about 2200 m^2 g^{-1}) with pore size predominantly in the range of 1–5 nm, while surface area of PAN/MWCNT samples was significantly lower (BET surface area 970 m^2 g^{-1}). The highest capacitance and energy density was obtained for PAN/SWCNT samples, suggesting SWCNT advantage in charge storage. The capacitance behavior of these electrodes has also been tested in ionic liquids, and the energy density in ionic liquid is about twice the value obtained using KOH electrolyte.

1. Introduction

The activated carbons have wide range of applications such as liquid/gas phase adsorptions [1–4], gas, water or element purification [5–7], catalyst support [8–11], energy storage [12–18] and many other applications due to high surface area, pore structure and adsorption capacity [19–21]. The pore structure of activated carbon depends on the precursor, activating agent as well as on process conditions. The precursors for activated carbons include polyacrylonitrile (PAN) [17,22–25], phenolic resin [18,22], petroleum coke [5,26], anthracite [27,28], pitch [29], coal [30–33], carbon nanotube(CNT)/carbon nanofiber (CNF) [13,34], and a number of natural fibers/shells [6,15,35,36].

There are two general approaches to modify carbon materials to increase its adsorption capacity. The first approach is to make use of gasifying agents like CO_2 [37–40] or water vapour [14,39–41] and is known as thermal or physical activation. The chemical activation using hydroxides, halides and acids is another approach for producing porous carbon. The chemical activating agents include KOH [5,23,26–28,34,42], NaOH [7,27,29,34,43], $ZnCl_2$ [22,36,44–46], H_3PO_4 [6,35,46], NH_4Cl, $FeCl_3$, and $AlCl_3$ [19,20,35,47]. The advantages of chemical activation over physical activation include higher carbon yield, lower activation time and temperature, and controlled pore size distribution.

Polyacrylonitrile, a carbonizing polymer, exhibits good interaction with carbon nanotubes [48–51]. A number of studies have been reported on PAN/CNT films and fibers [37,48–50,52–59]. Fibers have been spun by conventional solution spinning [48,49], gel spinning [50], as well as by electrospinning [53–55,57]. PAN/CNT based carbon fiber containing 1 wt.% carbon nanotube with respect to the weight of the polymer, can have 50% higher tensile strength than a carbon fiber processed without carbon nanotube [60]. Specific capacitance of a PAN/SWCNT film containing 40 wt.% SWCNT was as high as 380 F g^{-1} [37]. These studies clearly suggest the potential of PAN/CNT system for making both structural as well as porous carbon materials for a variety of applications. To the best of our knowledge, to date, there are no activation studies in the literature on solution spun PAN/CNT fibers. In this paper we report the structure, morphology, and electrochemical capacitor behavior of stabilized and CO_2 and KOH activated PAN and PAN/CNT fibers.

2. Experimental

The PAN and PAN/CNT fibers containing 5 wt.% CNT were solution spun by dry-jet-wet spinning using the previously described procedure [48,49]. SWCNTs were obtained from Carbon Nanotechnologies, Inc. (Houston, TX) (Grade P0247, 2.4% catalytic impurity) and MWCNTs were from Iljin Nanotech, Co. (Korea) (2.5% catalytic impurity). Diameter of the solution spun fibers was in the range of

* Corresponding author. Tel.: +1 404 894 2490; fax: +1 404 894 8780.
E-mail address: satish.kumar@gatech.edu (S. Kumar).

0378-7753/$ – see front matter © 2008 Elsevier B.V. All rights reserved.
doi:10.1016/j.jpowsour.2008.08.093

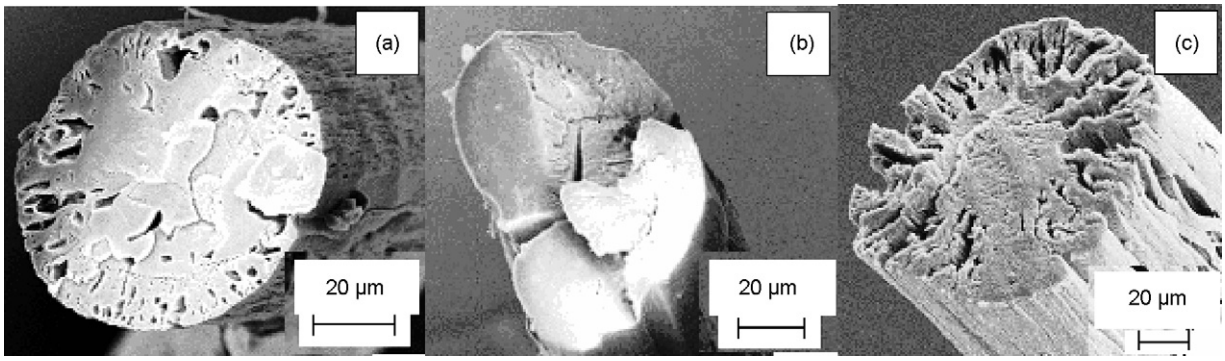

Fig. 1. Scanning electron micrographs of (a) PAN, (b) PAN/MWCNT and (c) PAN/SWCNT fibers stabilized for 16 h and boiled in DMF for 6 h.

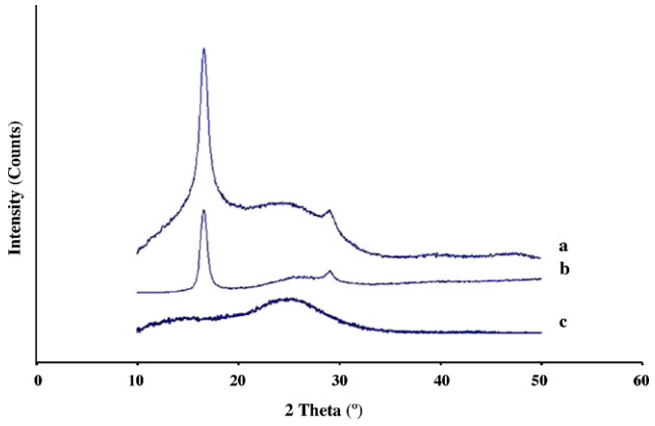

Fig. 2. WAXD scans for unstabilized and stabilized PAN fibers. Stabilization time: (a) 0 h, (b) 8 h, and (c) 16 h.

60–80 μm. All samples were stabilized without tension in a ceramic crucible in air by heating at 1 °C min^{-1} to 285 °C and by holding at that temperature for 2, 4, 8 and 16 h. To study the extent of stabilization, these samples were treated in dimethyl formamide (DMF) at 150 °C for 6 h to remove unstabilized PAN, and were examined by scanning electron microscopy as well as by wide angle X-ray diffraction (WAXD). As discussed in the subsequent section, all three samples used for carbonization and activation were stabilized for 16 h.

Samples stabilized for 16 h were carbonized by heating them from room temperature to 700 °C at 5 °C min^{-1}, and then holding for 1 h at 700 °C in argon in a Blue M Electric 1200 box furnace. These carbonized samples were physically activated at 900 °C in CO_2 for 1 h in the same furnace. For chemical activation, 16 h stabilized samples were immersed in 6 M KOH for 24 h at room temperature. KOH impregnated fibers were dried at 90 °C for 24 h in vacuum. With KOH impregnation, fiber weight increased by about a factor of two, and resulted in increased diameter. KOH impregnated fibers were heated at 5 °C min^{-1} to 800 °C and held at that temperature for 1 h in argon. KOH activated samples were cooled down to room temperature and repeatedly washed with hot distilled water to remove excess KOH. Therefore it should be noted that CO_2 activated samples were first carbonized and then activated, while the samples activated by KOH went from stabilization to activation, without the separate carbonization step. The activation temperature of 900 °C for CO_2 and 800 °C for KOH were chosen based on the literature reports as well as our own preliminary work [7,17,61,62].

The activated carbon fibers were crushed in mortar with a pestle and mixed with 20 wt.% polyvinylidene difluoride ($-CH_2-CF_2-$) binder (80:20, carbon:PVDF). The electrodes were prepared by compression molding the activated carbon/binder mixture at 140 °C, under ~0.6 GPa stress for 1 h. The samples were tested for specific capacitance, power density and energy density using Solartron Cell Test 1470 using the previously described procedure [37,63,64]. Only mass of the carbon electrodes was used in the calculations and mass of the binder was excluded. The test set up includes a two electrode cell where two active electrodes are separated by an insulating porous separator (Celgard 3400 microporous

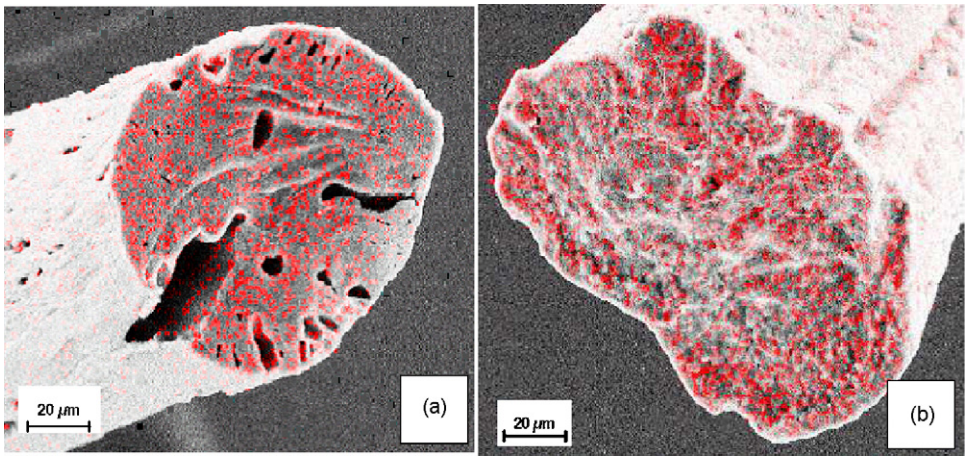

Fig. 3. Distribution of potassium through the fiber cross-section as characterized by energy dispersive system after impregnation of stabilized (a) PAN, and (b) PAN/MWCNT fibers in 6 M KOH for 24 h. Red dots indicate the presence of potassium.

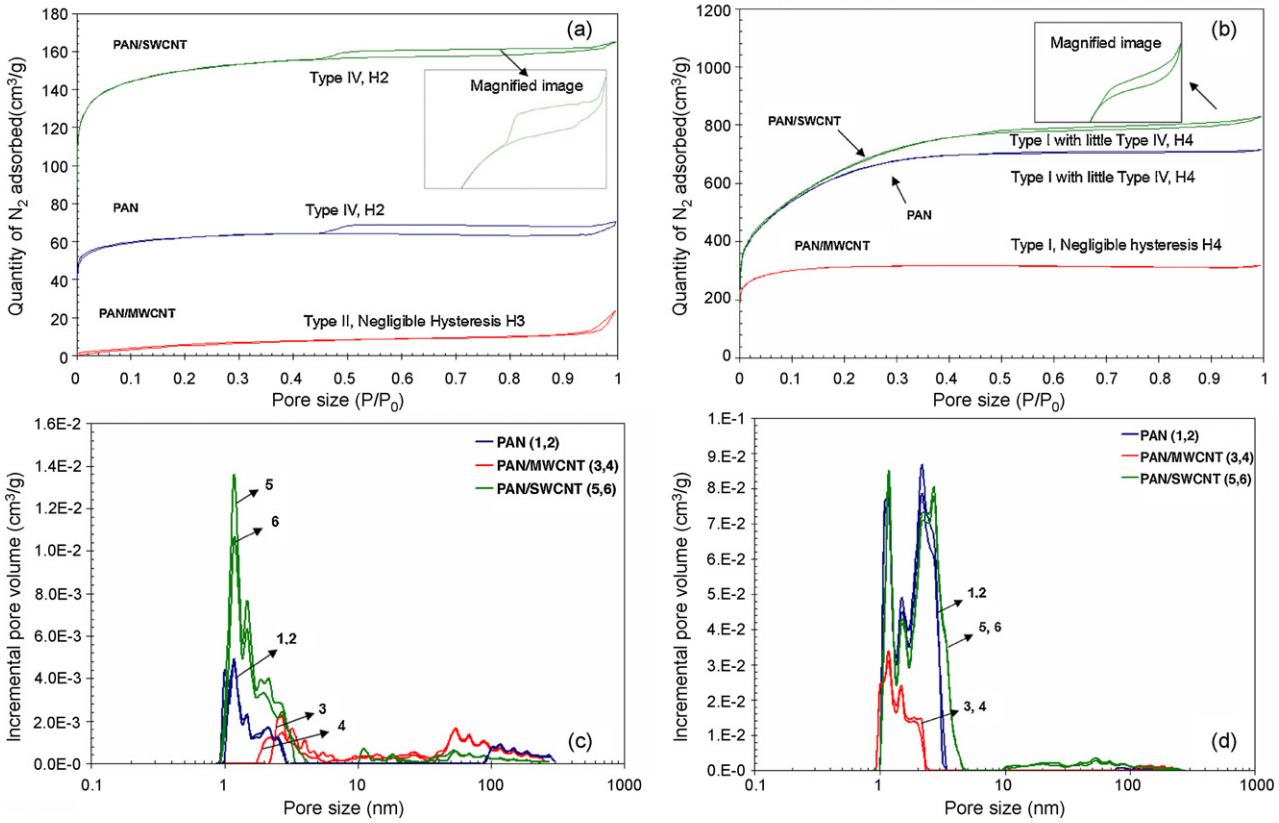

Fig. 4. Nitrogen adsorption isotherms (a and b) and pore size distribution measured by density functional theory method (c and d) for PAN, PAN/MWCNT and PAN/SWCNT fibers activated by (a and c) CO_2 and (b and d) KOH.

membrane) and sandwiched between two nickel current collectors. The electrode thickness varied between 100 and 300 μm, and the electrode diameter was about 0.5 cm. The electrolyte used for both galvanostatic and cyclic voltammetry (CV) tests was 6 M KOH as well as ionic liquid/organic electrolyte mixture of 1-butyl-3-methylimidazolium tetrafluoroborate ($BMIMBF_4$):acetonitrile (1:2 ratio). In the galvanostatic measurements, the cell was charged and discharged from 0 to 0.8 V for KOH electrolyte and from 0 to 3 V for ionic liquid, at constant current values of 0.1, 0.2, 0.5, 1, 2 and 5 mA. In CV measurements, scan rates of 5, 10, 20, 30, and 40 mV s^{-1} were used. The surface area and pore size distribution of the activated fibers were measured using nitrogen gas adsorption on Micromeritics ASAP 2020. Data was analyzed using BET and DFT methods [65–67]. Wide-angle X-ray diffraction (WAXD) studies were performed on a Rigaku Micromax-002 WAXS/SAXS system operated at 45 kV and 0.66 mA equipped with a Rigaku R-axis IV++ 2D detection system. The scanning electron microscopy (SEM) images were obtained on LEO SEM 1530. The dispersion of potassium in stabilized fibers was characterized using the energy dispersive system (EDS) in LEO SEM 1530. The impedance spectroscopy was performed on Potentiostat/Galvanostat (EG&G PAR Model 273A) in the frequency range of 100 mHz to 100 kHz using a two-electrode cell.

3. Results and discussion

PAN and PAN/CNT fibers stabilized for various times were treated in DMF for 6 h at 150 °C to monitor stabilization. Under these conditions, fiber diameters for samples stabilized for 2 and 4 h increased due to swelling of the unstabilized PAN, while fibers stabilized for 8 and 16 h did not show a significant change in diameter.

Table 1
Specific capacitance, surface area, and double layer capacity for CO_2 and KOH activated samples.

	Specific capacitance (F g^{-1}) (0.1 mA constant current test in 6 M KOH electrolyte)	Surface Area (m^2 g^{-1})		Double layer capacitance (μF cm^{-2})		Pore volume (cm^3 g^{-1})
		BET	DFT	BET	DFT	
CO_2 activation						
PAN	26	212	40	12	65	0.034
PAN/MWCNT (95/5)	21	30	10	70	210	0.035
PAN/SWCNT (95/5)	113	358	98	32	115	0.076
KOH activation						
PAN	172	2133	925	8	19	0.778
PAN/MWCNT (95/5)	134	970	316	14	42	0.234
PAN/SWCNT (95/5)	236	2266	916	10	26	0.936

The cross-sections of 16 h stabilized PAN and PAN/CNT fibers boiled in DMF for 6 h do not show a hollow core, which is consistent with complete stabilization (Fig. 1). Any unstabilized PAN remaining in the core would have been removed by DMF, leaving a hollow core as stabilization is controlled by diffusion of oxygen [68–70]. Stabilization progression in all samples was also monitored by WAXD [71]. Unstabilized and partially stabilized fibers show WAXD peak at $2\theta \sim 17^\circ$ due to (1 1 0) and (2 0 0) PAN reflections (Fig. 2), while this peak was absent in the 16 h stabilized samples. Based on these studies, it was concluded that only 16 h samples were fully stabilized. Therefore, for subsequent studies all three-fiber samples were stabilized for 16 h. The potassium distribution in the stabilized and KOH impregnated samples was monitored by EDS, and was found to be uniform through the fiber cross section (Fig. 3).

Surface area and pore size distribution of activated fibers are characterized by nitrogen gas adsorption. Based on the IUPAC classification, type I nitrogen gas adsorption isotherm is exhibited by micropores, while type IV isotherm is exhibited by mesoporous materials [65–67]. For CO_2 activated PAN and PAN/SWCNT fibers, the hysteresis loop at higher relative pressure indicate the presence of mesoporosity while microporous type I behavior is observed at low pressures (Fig. 4). The type H2 hysteresis is often attributed to disordered carbon with a distribution of pore sizes or shape not well defined. Thus, the steep region in the desorption part of CO_2 activated PAN and PAN/SWCNT fibers (Fig. 4a Inset) suggests the presence of disordered carbon or sample with wide pore size or shape distribution. The CO_2 activated PAN/MWCNT sample show type II sorption isotherm typically obtained for non-porous or macroporous absorbent with negligible hysteresis of type H3 at relatively high pressure.

The KOH activated PAN and PAN/SWCNT fibers show type I isotherm (Fig. 4b) with high nitrogen uptakes at relatively low pressures characteristic of micropores with small amount of type IV mesopores behavior presenting a hysteresis loop at relatively high pressures. The hysteresis loops obtained for KOH activated PAN and PAN/SWCNT fibers are of type H4, which is typically attributed to narrow slit shaped pores including pores in the micropore region [66]. Similar type I isotherm is obtained for KOH activated PAN/MWCNT fibers with negligible hysteresis loop H4. All three KOH activated samples show pores predominantly in the 1–5 nm range, while somewhat broader pore size distribution can be seen for the CO_2 activated samples (Fig. 4c). In fact for KOH activated PAN/MWCNTs, the pore size distribution is predominantly in the 1–3 nm range. Surface area, calculated by both BET and DFT methods, for the KOH activated samples is an order of magnitude higher than for the corresponding CO_2 activated samples (Table 1).

Constant current charge–discharge as well as CV plots for samples tested in 6 M KOH electrolyte are given in Fig. 5, and the specific capacitance as a function of current density is plotted in Fig. 6. Deviation from ideal rectangular shape at about 0.1 V in both CO_2 and KOH activated samples (Fig. 5b) can be due to the presence of surface functional groups making a pseudo-capacitance contribution. High ohmic drop observed in charge–discharge curves can be due to high internal resistance of the electrodes as well as due to the distributed resistance of the electrolyte in the pores of the electrode. KOH activated samples exhibit substantially higher capacitance over the CO_2 activated samples in 6 M KOH as well as in ionic liquid electrolytes (Figs. 6 and 7). In addition, in both types of activation, PAN/SWCNT shows higher capacitance than PAN and PAN/MWCNT samples. Capacitance of PAN/SWCNT sam-

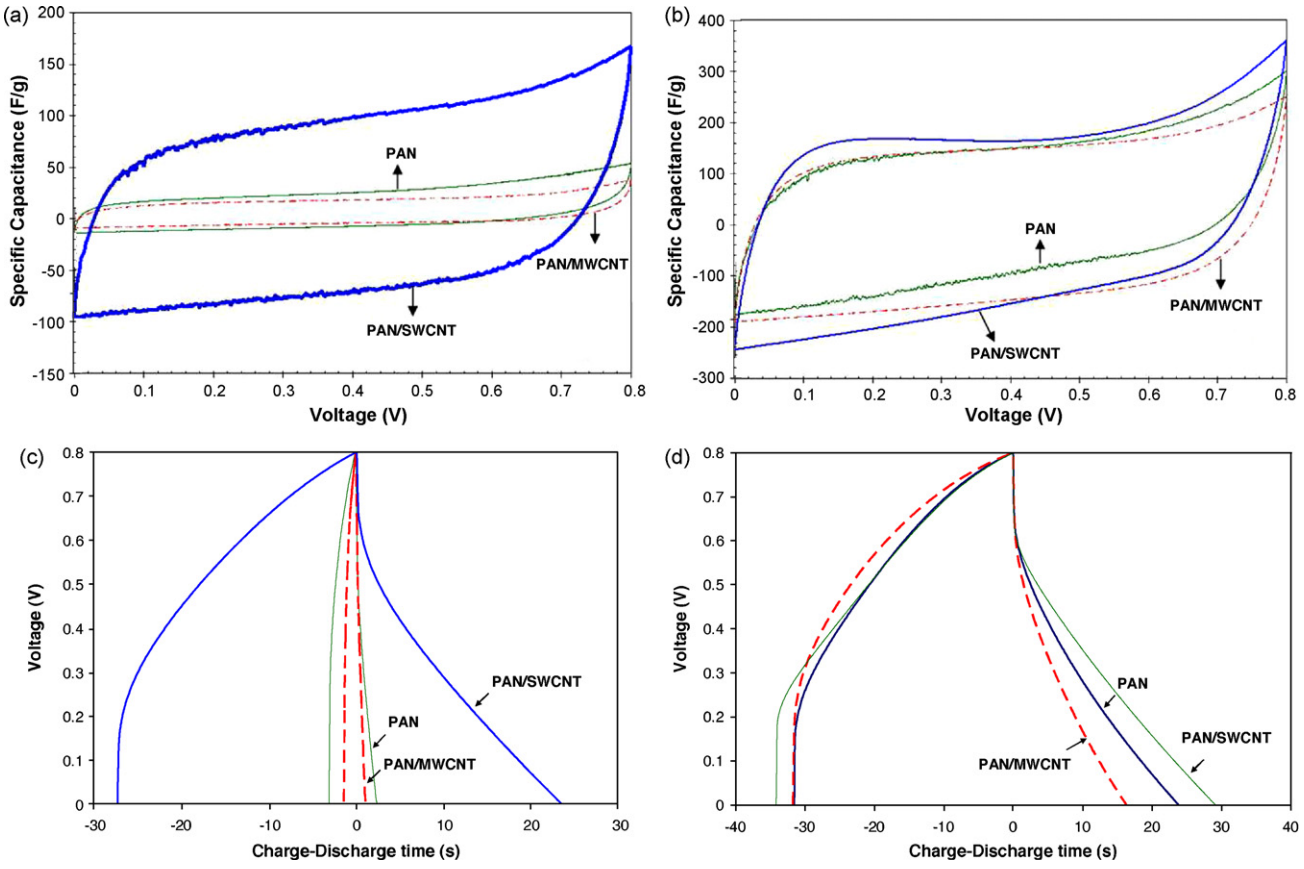

Fig. 5. The cyclic voltammograms at 5 mV s^{-1} scan rate (a and b) and charge discharge curves at a constant current test of 0.5 mA (c and d) for PAN, PAN/MWCNT and PAN/SWCNT fibers activated by (a and c) CO_2 and (b and d) KOH. The electrolyte for this test was 6 M KOH.

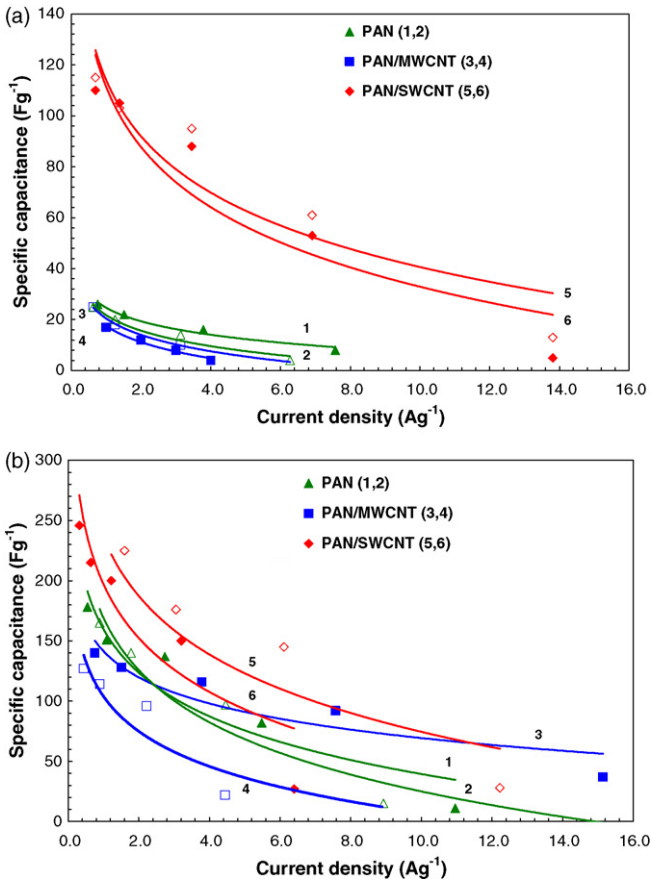

Fig. 6. The specific capacitance as a function of current density measured from constant current charge–discharge tests for PAN, PAN/MWCNT and PAN/SWCNT fibers activated by (a) CO_2 and (b) KOH. 6 M KOH was used as the electrolyte. In each case, two samples were tested to assess reproducibility.

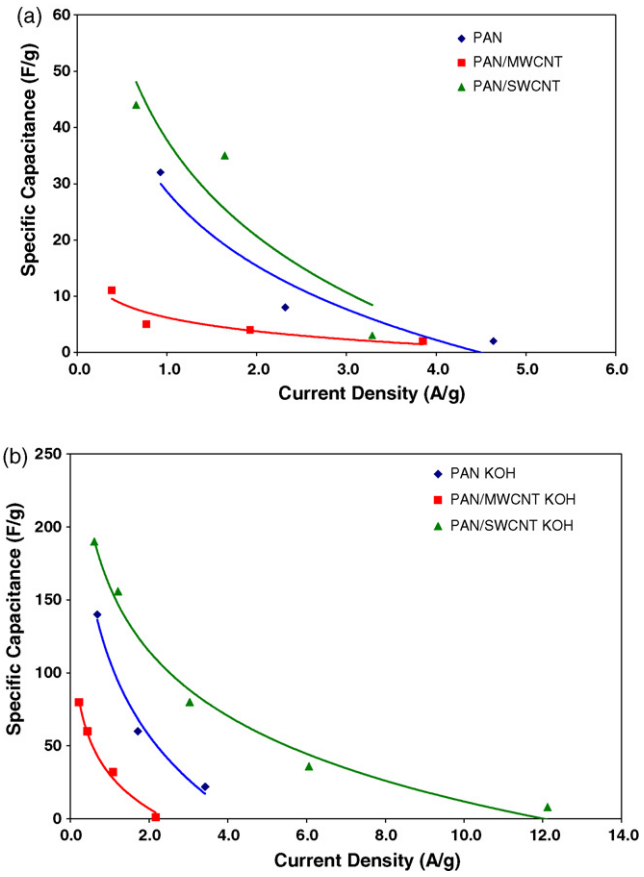

Fig. 7. The specific capacitance as a function of current density measured from constant current charge–discharge tests for PAN, PAN/MWCNT and PAN/SWCNT fibers activated by (a) CO_2 and (b) KOH. $BMIMBF_4$/acetonitrile (1:2) was used as the electrolyte.

ples activated in KOH is as high as 250 F g^{-1} at low current density (0.01 A g^{-1} in 6 M KOH). Energy density for KOH activated samples is also substantially higher than that for the CO_2 activated samples (Fig. 8). Energy density for KOH activated PAN/SWCNT is about 50% higher than the corresponding PAN and PAN/MWCNT. On the other hand, power density did not increase significantly even with the presence of conducting SWCNTs and MWCNTs. The energy density increased from 3 Wh kg^{-1} for KOH electrolyte to 6.4 Wh kg^{-1} in $BMIMBF_4$/acetonitrile electrolyte system for the chemically activated PAN/SWCNT (Fig. 8). However, the specific capacitance in ionic liquid is lower than that in KOH even at low current

Table 2
Summary of process conditions and properties for physical and chemical activation of PAN based precursor from literature as well as this work.

Group	Activation temperature (°C)	Precursor	Activation agent	BET surface area (m^2 g^{-1})	Specific capacitance (F g^{-1})
Physical activation					
Kim [77]	800	PAN electrospun fiber	Steam	~1160	133
Frackowiak [78]	800	Templated PAN	CO_2	~800	160
Ryu [39]	860	PAN based carbon fiber	Steam	~860	–
Wang [75]	900	PAN/SAN film	CO_2	~730	~165
Wang [75]	900	PAN electrospun fiber	CO_2	~306	~210
Zhou [63]	900	PAN/SAN/SWCNT films	CO_2	~130	~110
Liu [37]	700	PAN/SWCNT 60/40 films	CO_2	–	~380
This work	900	PAN/SWCNT fibers	CO_2	~358	~113

Group	M:C ratio*/molarity/%	Precursor	Activation agent	BET surface area (m^2 g^{-1})	Specific capacitance (F g^{-1})
Chemical activation					
Lee [79]	1–3:1	PAN fibers	KOH	~2500	–
Yue [22]	2:1	PAN coated fiber	$ZnCl_2$	~ 1600	–
Moon [7]	2 M	PAN fibers	KOH/NaOH	~1200/750	–
Lee [17]	1–3 M	PAN fibers	KOH	~2300	~ 180
Kim [80]	1–3%	Electrospun PAN fiber mat	$ZnCl_2$	~550	~ 140
Im[81]	2–6/4–8 M	Electrospun PAN fiber mat	$ZnCl_2$/KOH	~950/2400	–
This work	6 M	PAN, PAN/SWCNT fibers	KOH	~2200	~ 250

* M is K, Na, Zn etc. and C is carbon.

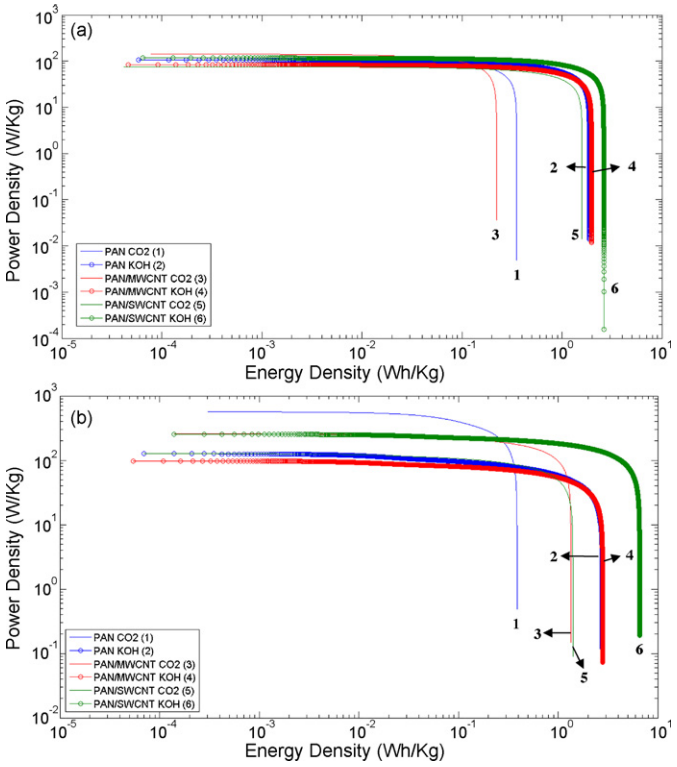

Fig. 8. The power density and energy density measured at 0.1 mA galvanostatic test using 6 M KOH(a) and $BMIMBF_4$/acetonitrile(1:2) (b) as electrolytes for PAN, PAN/MWCNT and PAN/SWCNT fibers activated by CO_2 and KOH.

density (Figs. 6 and 7). This is attributed to the relatively large ion size of the ionic liquid that cannot access small pores even at low current density. The bucky paper and carbonized PAN/CNT samples exhibit better wettability in ionic liquid than in KOH as determined by contact angle measurement [38].

The literature summary of activation conditions and capacitance performance for PAN based precursors is given in Table 2 for comparison with the current work. A surface area of 800–1000 $m^2\,g^{-1}$ and specific capacitance of 100–200 $F\,g^{-1}$ is typically reported for physically activated PAN films and fibers. A wide pore size distribution of 2–100 nm for films and nano fibers were reported. For chemically activated samples, surface area approaching 2500 $m^2\,g^{-1}$ is often reported. The surface area differences between the physically and chemically activated current set of samples is consistent with the literature reports. Table 3 summarizes capacitance data for other carbon materials, as well as for multi and single wall carbon nanotubes. The surface area differences between the CO_2 and KOH activated samples observed in the current work is consistent with the literature data that significantly higher surface area is obtained on chemical activation than physical activation.

Capacitance of both MWCNT and SWCNT electrodes is consistently below 100 $F\,g^{-1}$, while higher values have been reported for functionalized MWCNTs as well as for composites of carbon nanotubes with other systems (Tables 2 and 3). To the best of our knowledge, there are no previous literature reports on chemical activation of solution spun PAN/CNT fibers. Capacitance of 250 $F\,g^{-1}$ in the current study for KOH activated solution spun PAN/CNT fibers containing 5 wt.% SWCNTs in the precursor, is among the higher capacitance values reported to date. However, we do note that physically (CO_2) activated SWCNT/Polyacrylonitrile (PAN) composite film containing 40% SWCNTs showed capacitance in the range

Table 3
Surface area and electrochemical capacitance performance of various other carbon materials.

Group	Pore size	Carbon precursor	Electrolyte	BET surface area ($m^2\,g^{-1}$)	Specific capacitance ($F\,g^{-1}$)
Subnanometer, micro and meso porus carbons					
Chmiola [82]	< 1 nm	Chlorinated of carbide derived carbon	H_2SO_4	~1300	~140
Yamada [83]	<2 nm	Phenol formaldehyde based activated carbon	$LiClO_4$	~1302	~104
Lee [17]	<2 nm	PAN based carbon	KOH	~2312	~113
Fuertes [73]	2–10 nm	Polyfurfuryl alcohol based carbon	KOH	~1880	~200
Yamada [83]	2–50 nm	Phenol formaldehyde based activated carbon	$LiClO_4$	~1455	~119
Morishita [74]	2–30 nm	Polyvinyl alcohol based activated carbon with magnesium acetate/citrate	H_2SO_4	~1900	>300
This work	2–5 nm	PAN, PAN/SWCNT fibers	KOH	~2200	~250

Group	CNT type	Carbon nanotube treatment	Electrolyte	BET surface area ($m^2\,g^{-1}$)	Specific capacitance ($F\,g^{-1}$)
Carbon nanotubes					
Yoon [84]	MWCNT	As synthesized/NH_3 plasma treated	KOH	~10/87	~39/207
Zhang [85]	MWCNT	Aligned/entangled	$EMIBF_4$*	~111/283	~25/15
Shiraishi [86]	MWCNT	As synthesized/HCl treated	Et_4BF_4 **	~222/382	~24/15
Niu [87]	MWCNT	HNO_3 treated	H_2SO_4	~430	113
Chen [88]	MWCNT	HNO_3 treated	H_2SO_4	–	~365
Pan [89]	MWCNT	Tube in tube structure***	H_2SO_4	~500	~203
Futaba [90]	SWCNT	Densely packed SWCNT	Et_4NBF_4 **	~1000	< 15
Shiraishi [91]	SWCNT	HCl treated/thermal oxidation at 225 °C/5 h	$LiClO_4$	~780	~60
Liu [72]	SWCNT	Electrochemical treated with KOH	KOH	~110	~56
Zhou [38,64]	SWCNT	Untreated bucky paper	KOH	~540	~55
Zhou [38,64]	SWCNT	Untreated bucky paper	$BMIMBF_4$****	~ 540	~ 75
Zhou [38,64]	SWCNT	Aryl sulponic acid functionalized	$BMIMBF_4$****	~300	~105
Barisci [92]	SWCNT	Untreated/annealed up to 1050 °C	Ag/AgCl	~173/247	~36/14

* $EMIBF_4$ – 1-ethyl-3-methylimidazolium tetrafluoroborate.
** Et_4NBF_4 – tetraethylammonium tetrafluoroborate in propylene carbonate.
*** Tube in tube structure – templated MWCNTs (300 nm) were pyrolysed in ethylene at 900 °C to create tubular structures (30 nm) inside CNTs.
**** $BMIMBF_4$ – 1-butyl-3-methylimidazolium tetrafluoroborate in acetonitrile (1:1 ratio).

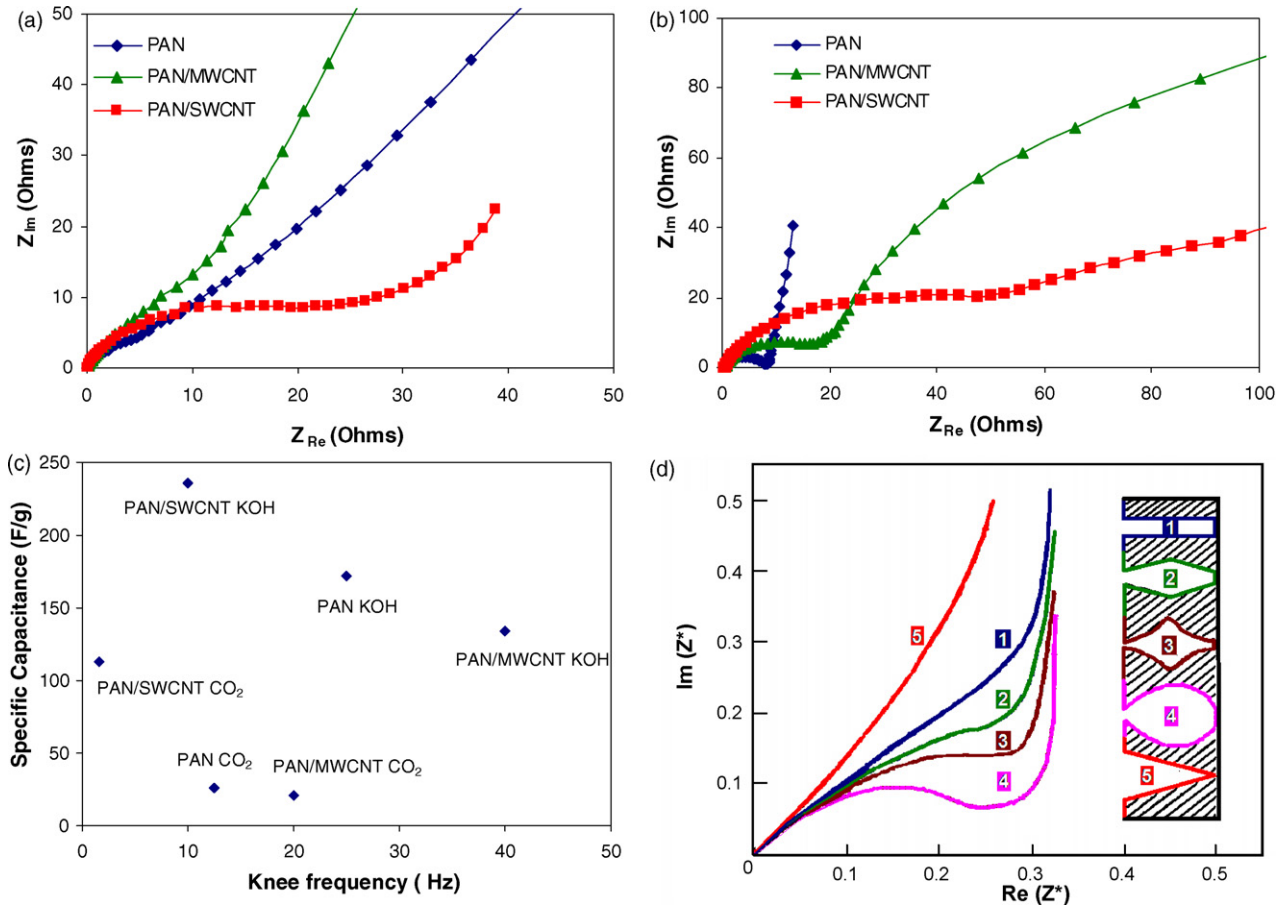

Fig. 9. Impedance spectroscopy results for PAN, PAN/MWCNT and PAN/SWCNT samples activated by (a) CO_2 and (b) KOH. (c) Specific capacitance plotted against knee frequency (d) Pore shapes treated by Keiser [76] and corresponding complex–plane impedance plots (Fig. 9d. is adapted from ref. [76]).

of 60–380 F g^{-1}, when the test cell was discharged from 0.7 to 0.2 V [37]. These studies show that the electrochemical capacitance of activated PAN/SWCNT composites is higher than that of either the SWCNT bucky paper or the activated PAN alone. Addition of just a few percent carbon nanotubes improves the capacitance performance significantly.

While there is no definite correlation established to date between the measured specific capacitance, electrolyte ion size, wettability and electrode pore distribution, most literature reports suggest that meso-pores represents the ideal pore size for electrochemical capacitors [38,72–75]. However, there is a recent report of anomalously high capacitance at sub-nanometer pore size. The pore size obtained by KOH activation in the current work (1–5 nm) measured using nitrogen adsorption is on the high end of the micropore size and at the lower end of the mesopore size. Sub-nanometer size pores could not be measured in the samples studied in the current work due to our instrumental limitation, and therefore we draw no conclusions on the anomalous mechanism.

Fig. 9 show impedance plots for CO_2 and KOH activated samples. The knee frequency, transition point between kinetics controlled high-frequency impedance and migration controlled low-frequency impedance, is a measure of electrical and ionic conductivity of the cell. Specific capacitance as a function of knee frequency shows that for a given series (KOH or CO_2 activation), samples with higher knee frequency have lower specific capacitance (Fig. 9c). However, it is noted that the CO_2 activated samples for a given knee frequency have lower specific capacitance than the KOH activated samples. Keiser [76] derived relations for impedance as a function of frequency for various pore geometries using a transmission line equivalent circuit (Fig. 9d). The impedance curves of CO_2 activated PAN and PAN/MWNT samples exhibiting low specific capacitance compare in shape to the Keiser plots for type 5 pores. The type 5 pores in Keiser plot are wider at the surface with a decreasing width as they go deeper in the sample. However, a comparison of the observed impedance data to the Keiser derived impedance data suggests that KOH activated samples as well as CO_2 activated PAN/SWNT samples contains pores of the type 2, 3 or 4 with narrow entrance and wider body, which can act as electrolyte reservoir.

In the case of CO_2 activation, pores are expected to have wider orifice on the surface that narrows down along the pore depth. This is due to CO_2 diffusion along the sample thickness. In single and multiwall carbon nanotube containing samples, CO_2 can also diffuse through hollow tube core, as well as through tube interstices in the case of SWCNT. In the case of SWNT, the single graphene layer would be easily damaged during CO_2 activation, providing pathways for CO_2 diffusion through the sample. While in the case of MWCNTs, due to the presence of multiple graphene layers, damage under CO_2 activation may be limited to few walls, while the other walls remain intact. Thus CO_2 diffusion through the bulk of the sample is very limited or non-existent in PAN/MWCNT samples, while it occurs in PAN/SWCNT samples. This is reflected in differences in surface area as well as in capacitance performance of the three CO_2 activated samples (Table 1). This also explains why impedance behavior and the pore shapes in PAN/SWCNT are of different type than in PAN and PAN/MWCNT.

Another question is why MWCNT contribute in a negative way to the capacitance behavior, as under both types of activation, PAN/MWCNT samples exhibit lower capacitance than the corresponding PAN. This can also be understood by multiple graphene layer stacking in MWCNTs, which is not always penetrated by CO_2 activation than the surrounding matrix. Hence, we hypothesize that the presence of MWCNTs limits activation, resulting in relatively low surface area and hence relatively low capacitance as compared to PAN and PAN/SWCNT. Interaction differences between PAN-SWCNT and PAN-MWCNT may also be responsible for some of the observed differences. Based on the temperature dependence of dynamic mechanical tan δ plots, differences between PAN/SWCNT and PAN/MWCNT interactions have indeed been reported previously [49]. Width of the tan δ vs temperature plot for the PAN/MWCNT fibers is significantly reduced as compared to that of the control PAN due to polymer interaction with the nanotubes resulting in narrower spectrum of relaxation times. In the case of SWCNT containing fibers, tan δ peak is broadened towards high temperature. We conjecture that PAN interactions with SWCNT are stronger than with other larger diameter MWCNTs and that PAN segments closer to the SWCNT exhibit tan δ loss at higher temperature than the segments farther from it, leading to the broadening in the high temperature region. Intercalation of PAN in the SWCNT bundle may also be partially responsible for the tan δ broadening behavior. Intercalated PAN on activation would enhance surface area leading to higher capacitance.

4. Conclusions

The structure, and electrochemical properties of PAN, PAN/SWCNT, and PAN/MWCNT fibers activated by physical (CO_2) and chemical (KOH) methods are compared. High specific capacitance, surface area, and pore volume with narrow pore size distribution are achieved in PAN/SWCNT with chemical activation. The specific capacitance of KOH activated PAN/SWCNT samples was as high as 250 F g^{-1} in 6 M KOH electrolyte. Under the comparable KOH activation conditions, PAN and PAN/SWCNT fibers had comparable surface areas (BET surface area about 2200 m^2 g^{-1}) with pore size predominantly in the range of 1–5 nm, while surface area of PAN/MWCNT samples was significantly lower (BET surface area 970 m^2 g^{-1}). The highest energy density was obtained for KOH activated PAN/SWCNT in ionic liquid.

Acknowledgement

This work is supported by the Air Force Office of Scientific Research. We are grateful to Professor Meilin Liu for the use of frequency response analyzer and to Beom-Jin Yoon for useful discussions.

References

[1] A. Ahmadpour, B.A. King, D.D. Do, Ind. Eng. Chem. Res. 37 (1998) 1329.
[2] Z. Hu, M.P. Srinivasan, Y. Ni, Carbon 39 (2001) 877.
[3] Y. Hattori, N. Noguchi, F. Okino, H. Touhara, Y. Nakahigashi, S. Utsumi, H. Tanaka, H. Kanoh, K. Kaneko, Carbon 45 (2007) 1391.
[4] D. Lozano-Castello, D. Cazorla-Amoros, A. Linares-Solano, D.F. Quinn, Carbon 40 (2002) 989.
[5] T. Otowa, Y. Nojima, T. Miyazaki, Carbon 35 (1997) 1315.
[6] N.H. Phan, S. Rio, C. Faur, L. Le Coq, P. Le Cloirec, T.H. Nguyen, Carbon 44 (2006) 2569.
[7] S.Y. Moon, M.-s. Kim, H.-S. Hahm, Y.-S. Lim, Mater. Sci. Forum 510–511 (2006) 750.
[8] M. Fan, P. Zhang, Energy Fuels 21 (2007) 633.
[9] A. Guha, W. Lu, T.A. Zawodzinski Jr., D.A. Schiraldi, Carbon 45 (2007) 1506.
[10] P.D. Tien, T. Satoh, M. Miura, M. Nomura, Energy Fuels 19 (2005) 2110.
[11] D.R. Rolison, Science 299 (2003) 1698.
[12] B.E. Conway, Plenum Press, New York, 1999, xxviii.
[13] S.-H. Yoon, S. Lim, Y. Song, Y. Ota, W. Qiao, A. Tanaka, I. Mochida, Carbon 42 (2004) 1723.
[14] F.-C. Wu, R.-L. Tseng, C.-C. Hu, C.-C. Wang, J. Power Sources 144 (2005) 302.
[15] V. Subramanian, C. Luo, A.M. Stephan, K.S. Nahm, S. Thomas, B. Wei, J. Phys. Chem. C 111 (2007) 7527.
[16] F.-C. Wu, R.-L. Tseng, C.-C. Hu, C.-C. Wang, J. Power Sources 159 (2006) 1532.
[17] J.-G. Lee, J.-Y. Kim, S.-H. Kim, J. Power Sources 160 (2006) 1495.
[18] H. Teng, Y.-J. Chang, C.-T. Hsieh, Carbon 39 (2001) 1981.
[19] R.C. Bansal, J.-B. Donnet, F. Stoeckli, Marcel Dekker, Inc. New York, 1988.
[20] J.-B. Donnet, R.C. Bansal, Marcel Dekker, Inc. New York, 1984.
[21] H. Marsh, F. 2006. Rodriguez-Reinoso, Activated Carbon, Elsevier Science Ltd., Oxford, 322.
[22] Z. Yue, C.L. Mangun, J. Econ. Carbon 40 (2002) 1181.
[23] M. Wu, Q. Zha, J. Qiu, Y. Guo, H. Shang, A. Yuan, Carbon 42 (2004) 205.
[24] M.S.A. Rahaman, A.F. Ismail, A. Mustafa, Polym. Degrad. Stab. 92 (2007) 1421.
[25] E. Fitzer, D.J. Muller, Carbon 13 (1975) 63.
[26] L. Chunlan, X. Shaoping, G. Yixiong, L. Shuqin, L. Changhou, Carbon 43 (2005) 2295.
[27] M.A. Lillo-Rodenas, D. Cazorla-Amoros, A. Linares-Solano, Carbon 41 (2003) 267.
[28] D. Lozano-Castello, M.A. Lillo-Rodenas, D. Cazorla-Amoros, A. Linares-Solano, Carbon 39 (2001) 741.
[29] J.A. Macia-Agullo, B.C. Moore, D. Cazorla-Amoros, A. Linares-Solano, Carbon 42 (2004) 1367.
[30] A. Ahmadpour, D.D. Do, Carbon 34 (1996) 471.
[31] P. Ehrburger, A. Addoun, F. Addoun, J.-B. Donnet, Fuel 65 (1986) 1447.
[32] M.J. Illan-Gomez, A. Garcia-Garcia, C. Salinas-Martinez de Lecea, A. Linares-Solano, Energy Fuels 10 (1996) 1108.
[33] H. Teng, L.Y. Hsu, Ind. Eng. Chem. Res. 38 (1999) 2947.
[34] E. Raymundo-Pinero, P. Azais, T. Cacciaguerra, D. Cazorla-Amoros, A. Linares-Solano, F. Beguin, Carbon 43 (2005) 786.
[35] A. Huidobro, A.C. Pastor, F. Rodriguez-Reinoso, Carbon 39 (2001) 389.
[36] T. Yang, A.C. Lua, Mater. Chem. Phys. 100 (2006) 438.
[37] T. Liu, T.V. Sreekumar, S. Kumar, R.H. Hauge, R.E. Smalley, Carbon 41 (2003) 2440.
[38] C. Zhou, PhD Thesis, Georgia Institute of Technology, 2006, 42.
[39] Z. Ryu, H. Rong, J. Zheng, M. Wang, B. Zhang, Carbon 40 (2002) 1144.
[40] Tse-Hao Ko, W.-S. Kuo, C.-H. Hu, J. Appl. Polym. Sci. 81 (2001) 1090.
[41] P.H. Wang, Z.R. Yue, J. Liu, J. Appl. Polym. Sci. 60 (1996) 923.
[42] R. Xue, Z. Shen, Carbon 41 (2003) 1862.
[43] D. Lozano-Castello, J.A. Macia-Agullo, D. Cazorla-Amoros, A. Linares-Solano, M. Muller, M. Burghammer, C. Riekel, Carbon 44 (2006) 1121.
[44] F. Caturla, M. Molina-Sabio, F. Rodriguez-Reinoso, Carbon 29 (1991) 999.
[45] J. Ganan-Gomez, A. Macias-Garcia, M.A. Diaz-Diez, C. Gonzalez-Garcia, E. Sabio-Rey, Appl. Surf. Sci. 252 (2006) 5976.
[46] Y. Nakagawa, M. Molina-Sabio, F. Rodriguez-Reinoso, Microporous Mesoporous Mater. 103 (2007) 29.
[47] H. Marsh, F. Rodriguez-Reinoso, 2006.
[48] T.V. Sreekumar, T. Liu, B.G. Min, H. Guo, S. Kumar, R.H. Hauge, R.E. Smalley, Adv. Mater. 16 (2004) 58.
[49] H.G. Chae, T.V. Sreekumar, T. Uchida, S. Kumar, Polymer 46 (2005) 10925.
[50] H.G. Chae, M.L. Minus, S. Kumar, Polymer 47 (2006) 3494.
[51] T. Uchida, S. Kumar, J. Appl. Polym. Sci. 98 (2005) 985.
[52] T.V. Sreekumar, S. Kumar, US Patent 6,852,410, 2005.
[53] F. Ko, Y. Gogotsi, A. Ali, N. Naguib, H. Ye, G.L. Yang, C. Li, P. Willis, Adv. Mater. 15 (2003) 1161.
[54] H. Ye, H. Lam, N. Titchenal, Y. Gogotsi, F. Ko, Appl. Phys. Lett. 85 (2004) 1775.
[55] S. Prilutsky, E. Zussman, Y. Cohen, Nanotechnology 19 (2008) 165603.
[56] L. Vaisman, E. Wachtel, H.D. Wagner, G. Marom, Polymer 48 (2007) 6843.
[57] D.-K. Kim, S.H. Park, B.C. Kim, B.D. Chin, S.M. Jo, D.Y. Kim, Macromol. Res. 13 (2005) 521.
[58] F. Béguin, K. Szostak, G. Lota, E. Frackowiak, Adv. Mater. 17 (2005) 2380.
[59] H. Hou, J.J. Ge, J. Zeng, Q. Li, D.H. Reneker, A. Greiner, S.Z.D. Cheng, Chem. Mater. 17 (2005) 967.
[60] H.G. Chae, M.L. Minus, A. Rasheed, S. Kumar, Polymer 48 (2007) 3781.
[61] S. Jagannathan, PhD Thesis (in progress), Georgia Institute of Technology.
[62] J. Lee, J. Kim, S. Kim, J. Mater. Sci. 42 (2007) 2486.
[63] C. Zhou, T. Liu, T. Wang, S. Kumar, Polymer 47 (2006) 5831.
[64] C. Zhou, S. Kumar, C.D. Doyle, J.M. Tour, Chem. Mater. 17 (2005) 1997.
[65] S. Lowell, J.E. Shields, M.A. Thomas, M. Thommes, Characterization of Porous Solids and Powders: Surface Area, Pore Size and Density, Kluwer Academic Publishers, Dordrecht/Boston/London, 2004.
[66] K.S.W. Sing, D.H. Everett, R.A.W. Haul, L. Moscou, R.A. Pierotti, J. Rouquerol, T. Siemieniewska, Pure Appl. Chem. 57 (1985) 603.
[67] P.A. Webb, C. Orr, Analytical Methods in Fine Particle Technology, Micromeritics Instruments Corp., Norcross, Georgia, 1997.
[68] M.-J. Yu, C.-G. Wang, Y.-J. Bai, M.-X. Ji, Y. Xu, Polym. Bull. 58 (2007) 933.
[69] G.K. Layden, Carbon 10 (1972) 59.
[70] F.R. Barnet, M.K. Norr, Composites 7 (1976) 93.
[71] M.-J. Yu, Y.-J. Bai, C.-G. Wang, Y. Xu, P.-Z. Guo, Mater. Lett. 61 (2007) 2292.
[72] C.G. Liu, H.T. Fang, F. Li, M. Liu, H.M. Cheng, J. Power Sources 160 (2006) 758.
[73] A.B. Fuertes, G. Lota, T.A. Centeno, E. Frackowiak, Electrochim. Acta 50 (2005) 2799.
[74] T. Morishita, Y. Soneda, T. Tsumura, M. Inagaki, Carbon 44 (2006) 2360.
[75] T. Wang, PhD Thesis, Georgia Institute of Technology, 2007.

[76] H. Keiser, K.D. Beccu, M.A. Gutjahr, Electrochim. Acta 21 (1976) 539.
[77] C. Kim, Y. Kap-Seung, L. Wan-Jin, Electrochem. Solid-State Lett. 7 (2004) A397.
[78] E. Frackowiak, G. Lota, J. Machnikowski, C. Vix-Guterl, F. Beguin, Electrochim. Acta 51 (2006) 2209.
[79] Y.-J. Lee, J.-H. Kim, J. Kim, D.B. Lee, J.-C. Lee, Y.-J. Chung, Y.-S. Lim, Mater. Sci. Forum 449–452 (2004) 217.
[80] C. Kim, B.T.N. Ngoc, K.S. Yang, M. Kojima, Y.A. Kim, Y.J. Kim, M. Endo, S.C. Yang, Adv. Mater. 19 (2007) 2341.
[81] J.S. Im, S.-J. Park, Y.-S. Lee, J. Colloid Interface Sci. 314 (2007) 32.
[82] J. Chmiola, G. Yushin, Y. Gogotsi, C. Portet, P. Simon, P.L. Taberna, Science 313 (2006) 1760.
[83] H. Yamada, I. Moriguchi, T. Kudo, J. Power Sources 175 (2008) 651.
[84] B.-J. Yoon, S.-H. Jeong, K.-H. Lee, H. Seok Kim, C. Gyung Park, J. Hun Han, Chem. Phys. Lett. 388 (2004) 170.
[85] H. Zhang, G. Cao, Y. Yang, Z. Gu, J. Electrochem. Soc. 155 (2008) K19.
[86] S. Shiraishi, M. Kibe, T. Yokoyama, H. Kurihara, N. Patel, A. Oya, Y. Kaburagi, Y. Hishiyama, Appl. Phys. A: Mater. Sci. Process. 82 (2006) 585.
[87] C. Niu, E.K. Sichel, R. Hoch, D. Moy, H. Tennent, Appl. Phys. Lett. 70 (1997) 1480.
[88] Q.-L. Chen, K.-H. Xue, W. Shen, F.-F. Tao, S.-Y. Yin, W. Xu, Electrochim. Acta 49 (2004) 4157.
[89] H. Pan, C.K. Poh, Y.P. Feng, J. Lin, Chem. Mater. 19 (2007) 6120.
[90] D.N. Futaba, K. Hata, T. Yamada, T. Hiraoka, Y. Hayamizu, Y. Kakudate, O. Tanaike, H. Hatori, M. Yumura, S. Iijima, Nat. Mater. 5 (2006) 987.
[91] S. Shiraishi, H. Kurihara, K. Okabe, D. Hulicova, A. Oya, Electrochem. Commun. 4 (2002) 593.
[92] J.N. Barisci, G.G. Wallace, D. Chattopadhyay, F. Papadimitrakopoulos, R.H. Baughman, J. Electrochem. Soc. 150 (2003) E409.